Shallow and Intermediate Water Wave Energy Converter

Ramuel T. Maramara[#1], Masoud Masoumi[#2]

[#]*Brimes Energy Inc*
1347 Lincoln Ave #9, Holbrook, NY 11741
[1]rmaramara@brimesenergy.com
[2]mmasoumi@brimesenergy.com

Abstract **This paper represents both an analytical formulation and a series of experimental testings for a flap-type seabed-mounted WEC. The analytical modeling provides an insight into the parameters affecting the design and optimization for the maximum power output. Experimental testings in the wave flume are designed to study the effects of damping due to the PTO mechanism on both power output and efficiency of the device.**

Keywords **— Wave Energy Converter, Mathematical Modeling, Numerical Simulation, Wave Flume Testing**

I. Introduction

The estimation of total available wave power of 2.7 TW, which exceeds global consumption of electricity, provides a great incentive for technologies capable of efficiently generating power from this untapped source of energy [1, 2]. The wave energy converter (WEC) described in this paper has been developed and is currently going through rigorous laboratory tests. However, the purpose of this paper is to provide a simple yet practical dynamic model for the system, the way it interacts with waves, and some experimental testings for power output estimation. Fig. 1 shows a schematic representation of this flap-type wave energy converter designed for shallow and intermediate depth (SID) water types, called *Jellyfish*.

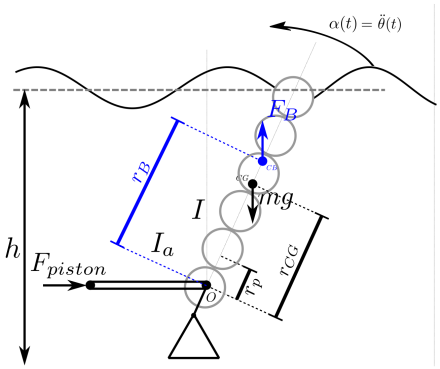

Fig. 1 Free body diagram showing hydrodynamic and hydrostatic forces for the prototype prototype

The final design of the system is basically a flap-type structure hinged at the bottom of the sea with the flap part designed close to the Salter's duck profile [3] and a hydraulic power-take-off (PTO) mechanism.

II. Mathematical Formulation

The equation of motion for the device can be written as

$$\left(I+I_a\right)\ddot{\theta}(t)+C_r\dot{\theta}(t)+K\theta=T_{exc}-T_{pto} \tag{1}$$

where, I and I_a are the pod and added moment of inertia respectively, C_r is the radiation damping, K represents stiffness coefficient, T_{exc} is the excitation torque, and T_{pto} is the torque created by PTO mechanism. The excitation torque is caused by a summation of incident and scattered waves while added inertia is related to the force caused by the mass of water. Radiation damping is the representative of power exchanged between the sea and the body. Both buoyancy force and gravity are considered as hydrostatic forces (see Fig. 1).

We further develop the equation of motion by replacing the force from the piston configuration. This force is a function of pressure values, P_A and P_B, and areas on both sides of the piston inside the cylinder, A_{cap} and A_{rod}. The pressure values can be written as a function of dynamic viscosity μ, linear velocity of the piston inside the cylinder in either direction, and half stroke length values in each direction, L_A and L_B. Final force equation for the piston can be represented as

$$F_{piston}=\mu r_p\left(\frac{A_{cap}}{L_B}-\frac{A_{rod}}{L_A}\right)\dot{\theta}(t) \tag{2}$$

and since $T_{pto}=r_p\times Fpiston$, we can find power take-off torques as

$$T_{pto}=\mu r_p^2\left(\frac{A_{cap}}{L_B}-\frac{A_{rod}}{L_A}\right)\dot{\theta}(t) \tag{3}$$

From Eqs.(1)-(3), the equation of motion for this system can be derived as follows

$$\begin{aligned}\left(I+I_a\right)\ddot{\theta}(t)+\left[C_r+\mu r_p^2\left(\frac{A_{cap}}{L_B}-\frac{A_{rod}}{L_A}\right)\right]\dot{\theta}(t)\\ +K\theta(t)=T_{exc}\end{aligned} \tag{4}$$

Both radiation damping and added inertia variables are functions of frequency of the excitation. These values can be calculated using boundary element method (BEM). For a design

with a rectangular flap as an estimation to our prototype with parameters listed in Table 1, radiation damping and added inertia values can be calculated using OpenWEC software, which basically is an open source code that uses NEMOH [4], another open source BEM solver.

Table 1 Prototype properties (all values have SI unit)

Width	Height	Length	Water Depth	Density
0.1143	0.6858	1.03024	0.9144	260.71

Resonant frequency of the system can then be found as

$$\omega_n = \sqrt{\frac{K}{I + I_a(\omega)}} \tag{5}$$

in which, I_a is a function of excitation frequency. Consider the prototype shown in Fig. 1; it has six hollow PVC cylinders, each with the inner diameter of 4 in and outer diameter of 4.5 in. Two steel bars on one side are used to support the cylinders and also there is a 3.75" distance between the rotating axis and the center of the lowest cylinder. Each cylinder can be filled with water up to 17.637 lbs (8 Kg).

To study the effects of mass and its distribution on natural frequency of the device, five different cases were considered. The results along with these cases are shown in Fig. 2. Here, value K has been estimated using $K = \rho_w g t^3 d/12 + (\rho_w - \rho_f) g t d h^2/2$, where ρ_w and ρ_f are the water and device densities, t is the thickness, h is the water depth, and d stands for width of the flap, also g represents the acceleration of gravity [5]. To have a better understanding of a full scale device, results are scaled for a $1/20^{th}$ scale machine using Froude's law since the inertia forces are predominant. Also, spectra of the fully-developed sea-state is shown on the same plot simulated using Pierson-Moscowitz model [6] for different wind speed value, U.

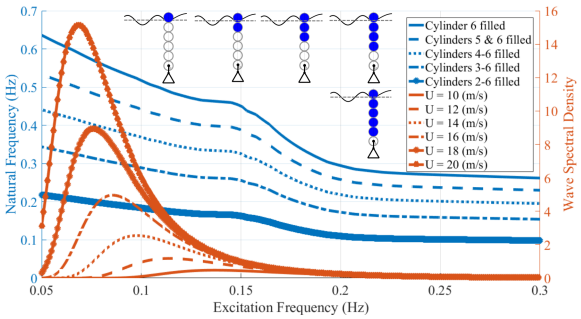

Fig. 2 Natural frequency changes for five different mass distributions along with the wave spectral density for a fully-developed sea-state for some wind speed (U) values

III. Experimental Setup

The objective for these series of experiments conducted on the $1/20^{th}$ scale prototype is to both study the effects of oil pressure on hydraulic PTO mechanism and find the optimal PTO force applied to the system for maximum efficiency in the face of waves with different time periods. For these tests, the flap-type bottom-mounted WEC has properties described in Table 1 and the hydraulic circuit setup is shown in Fig. 3. To control the oil pressures, three tanks with pressurized oil are used. Tank A is the reservoir and its pressure is always kept on 5 psi. Tanks B and C control the oil pressure for two different motions in the system. When the flap is moving in the same direction as incident waves, the pistons inside the cylinders installed on both sides of the flap move from left to right. The pressure on the left side of each cylinder that controls the damping for this motion is set using tank B. And once the flap is moving in the opposite direction of the incident waves, going back towards its initial position, damping force due to the PTO mechanism is controlled by the oil pressure in tank C.

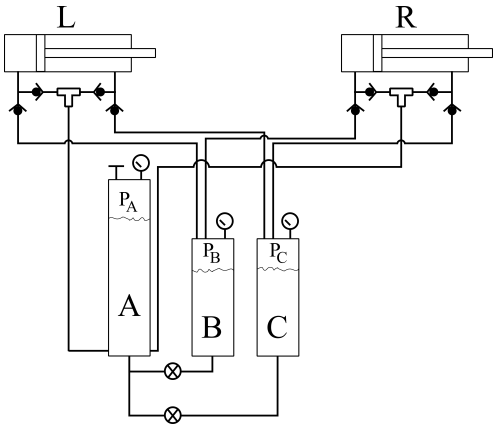

Fig. 3 A Schematic diagram of hydraulic circuit for the experimental setup showing tanks A, B, and C and cylinder-piston PTO installed on both right and left sides of the flap.

The flap is hinged at the bottom of the wave flume to a $31\times40\times7$ in^3 concrete plate and 3 in of it is out of the water above the surface. Water depth was kept 36 in throughout all these tests and the waves had 6 in height. Wave periods vary from 1 to 3 s with 0.5 s steps. For each test, 25 wave cycles were run in the wave tank. Pressure in tank B and tank C varies from 10 psi to 60 psi and 20 psi to 60 psi respectively. The diameter of all three oil tanks were 4 in. These values were chosen based on the capabilities of our in-house wave tank for experimental testing. Finally, it is worth mentioning that the prototype here is $1/20^{th}$ of the final device size. Fig. 4 shows a schematic diagram of the wave tank and the prototype inside for testing.

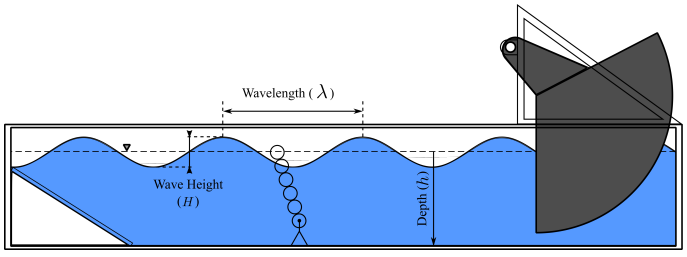

Fig. 4 A schematic diagram of the wave tank with the prototype installed (not to scale)

IV. Results & Discussion

Oil displacements in tanks B and C after 25-cycle waves were measured and then the power was calculated from the total time and pressure values. In the mathematical form, $Power = \frac{work}{time} = \frac{force \times displacement}{time} = \frac{(pressure \times area) \times displacement}{time}$. Fig. 5 shows the output power for the pressure values in tanks B and C when the waves with 1.5 s time period were used to test the prototype.

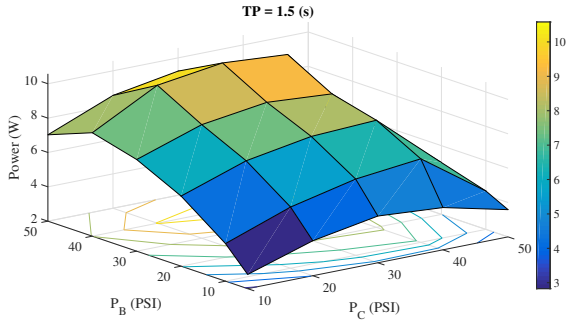

Fig. 5 Power extracted after 25 cycles of the waves with 1.5 s time period and 6 in height.

As it can be seen, there clearly exists an optimal power output for specific tank pressures. For this time period, the maximum power occur at P_C = 30 psi and P_B = 40 psi which is 10.58 W. Similar procedure was followed for the waves with time periods mentioned in the previous section to find the maximum power output and the corresponding pressure values in tank B and C. Results are shown in Fig. 6. In this figure, hollow circles represent the projections of data points on different planes to help identify the location of each point in the 3D plot. The subset in the figure is a top view of the graph for a better representation of pressure values in tanks and how they correspond to the power values. Maximum power output was found at P_C = 30 psi and P_B = 50 psi with the value of 11.84 W.

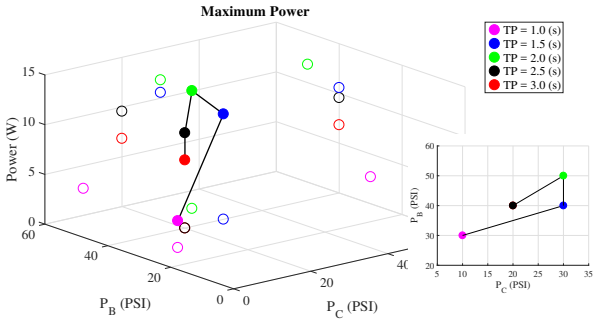

Fig. 6 Maximum power extracted after 25 cycles of the waves with 6 in height.

Since the final WEC will have a hydraulic system with only one set oil pressure, the ratio between pressure values can be found to help with the design. Pressure correspond to the force applied. Once the best pressure ratio for the PTO is found, then the area for both sides of the pistons can be designed in a way to provide such ratio in the PTO force.

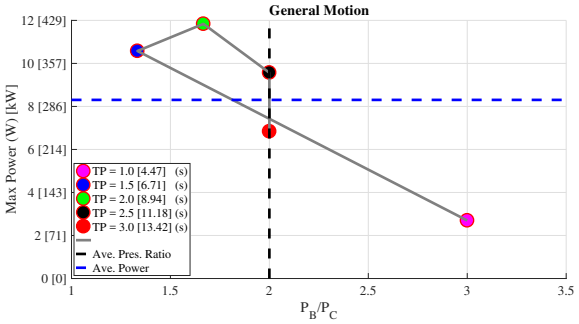

Fig. 7 Maximum power extracted after 25 cycles of waves with various time periods at different pressure ratios.

Fig. 7 shows the maximum power output values for different wave periods. However, it is represented based on the ratios between pressures in tanks B and C. In this figure, numbers in bracket are the scaled values for the $1/20^{th}$ scale device. For this device, the average power output is more than 8 W in the face of waves with periods from 1 to 3 s. The average pressure value to find the maximum power output for waves in this period range is $\frac{P_B}{P_C} = 2$.

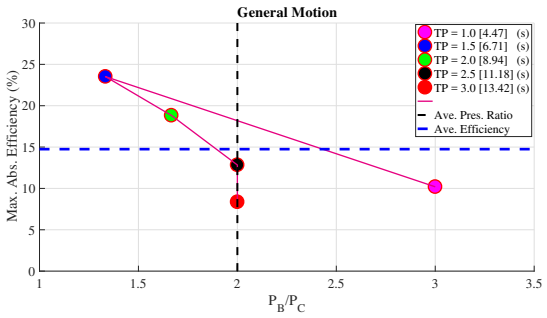

Fig. 8 Capture efficiency for various time periods at different pressure ratios.

Finally, the efficiency of the prototype can be calculated based on the energy flux of the incident waves and the output power. Energy per unit time and unit width of wave frontage (or energy flux) can be found from [7]

$$J = \frac{\rho g^2 D(kh)}{32\pi} T H^2 \tag{6}$$

where, k is the wave number, T is the time period of the wave, and H is the wave height. Also, $D(kh)$ is the depth function defined as

$$D(kh) = \left[1 - \left(\frac{\omega^2}{gk}\right)\right] kh + \frac{\omega^2}{gk} \tag{7}$$

Therefore, the capture efficiency of the WEC can be calculated. The results are shown in Fig. 8. Although the maximum power output was found for 2 s time period, the maximum efficiency of the device occur for waves with 1.5 s time period. On average and for this range of wave periods, the capture efficiency is about 15%. It is worth mentioning that this efficiency is for a prototype which was not optimized in terms of its natural frequency.

V. Comments & Conclusions

In this paper, analytical investigations were used to provide a general view about the various design parameters that affect the resonant frequency of the device. Natural frequency of the device can be controlled using fillable compartments as part of the design. These compartments can also be used for storm protection to sink the flap during the stormy weather condition.

A series of experimental tests were designed and conducted on a $1/20^{th}$ scale device to study the effects of damping caused by oil pressure in the hydraulic circuit. Optimal power values for each tank and the converter were recorded for waves with time periods vary from 1 s to 3 s. The maximum power output occurred at 2 s time period and the average ratio between pressures in tank B and tank C to get the maximum power output for this time period range was about 2. Since the pressure and force are correlated, this value can be used to design the piston areas. To design the device for a specific site or environment, pressure ratios in hydraulic circuit and the natural frequency of the machine can be optimized. For waves with the height of about 10 ft in a depth of 60 ft water, this device can reach up to %15 water-to-oil efficiency for wave periods between 4.47-13.42 s with non-optimized natural frequency.

Acknowledgements

The authors would like to thank the support of New York State Research and Development Authority (NYSERDA) and Clean Energy Business Incubator Program (CEBIP) at Stony Brook University.

References

[1] J. D. Isaacs and W. R. Schmitt, "Ocean energy: forms and prospects," *Science*, vol. 207, no. 4428, pp. 265–273, 1980.

[2] A. Pecher and J. P. Kofoed, *Handbook of Ocean Wave Energy*. Springer, 2017.

[3] S. Salter, D. Jeffrey, and J. Taylor, "Wave power-nodding duck wave energy extractors," *Energy from the oceans fact or fantasy*, pp. 5–8, 1976.

[4] A. Babarit and G. Delhommeau, "Theoretical and numerical aspects of the open source bem solver nemoh," in *11th European Wave and Tidal Energy Conference (EWTEC2015)*, 2015.

[5] H.-t. Zhao, Z.-l. Sun, C.-l. Hao, and J.-f. Shen, "Numerical modeling on hydrodynamic performance of a bottom-hinged flap wave energy converter," *China Ocean Engineering*, vol. 27, no. 1, pp. 73–86, 2013.

[6] W. J. Pierson and L. Moskowitz, "A proposed spectral form for fully developed wind seas based on the similarity theory of sa kitaigorodskii," *Journal of geophysical research*, vol. 69, no. 24, pp. 5181–5190, 1964.

[7] Y. Goda, *Random seas and design of maritime structures*. World Scientific Publishing Company, 2010, vol. 33.